Computational and structural insights into the pre- and post-hydrolysis states of multidrug resistance associated protein 1 in lipid bilayer membranes

Ágota Tóth*, Veronica Crespi, Angelika Janaszkiewicz, and Florent Di Meo*

Inserm UMR 1248 Pharmacology & Transplantation, Univ. Limoges, 2 rue du Prof. Descottes, 87000 F-Limoges, France

Contact information
Dr. Florent Di Meo & Ágota Tóth
Inserm U1248 Pharmacology & Transplantation, Univ. Limoges,
2 rue du Prof. Descottes,
87000 F-Limoges, France
florent.di-meo@inserm.fr, agota.toth@unilim.fr
Tel: +33(0)5 19 56 42 76

Abstract

ABC C-family drug membrane transporters play an important role in local pharmacokinetics, i.e., drug concentration in cellular compartments. From the structural point of view, only the bovine ortholog of the multidrug-resistance associated protein 1 have been resolved. We here used μs-scaled MD simulations to investigate the structure and dynamics of *b*MRP1 in pre- and post-hydrolysis functional states. The present work aims to investigate the slight but likely relevant structural differences between pre- and post-hydrolysis states of OF conformations as well as the interactions between MRP1 and surrounding lipid molecules. Global conformational dynamics show unfavourable extracellular opening associated with NBD dimerization indicating that the post-hydrolysis state adopts a close-conformation rather than an outward-open conformation. our present MD simulations also strengthen the expected active role of surrounding lipid in the allosteric communication between distant domain of MRP1 transporter. Furthermore, PE lipids in the inner leaflet as well as cholesterol in the so-called Cholesterol recognition amino acid consensus (CRAC) or inverted (CARC) motifs are expected to be key in MRP1 function.

Keywords. ABCC1/MRP1, molecular dynamics, pre/post-hydrolysis state, lipid-protein interplay, Drug Transporters

1. Background

Except for a few members[1–4], eukaryotic ATP-binding cassette (ABC) superfamily proteins are membrane transporters involved in efflux events, *i.e.*, they translocate a myriad of chemically different substrates across the membrane out of cells[1,5]. Among them, the ABCC family plays an active role in pharmacology by transporting xenobiotics such as anionic compounds including glucuro- and sulfo-conjugates[1,6,7]. The so-called multidrug resistance-associated proteins (MRPs) were reported as of importance by the International Transporter Consortium (ITC)[8] which has stressed[5] that particular attention must be paid when they are suspected to be major determinants of drug disposition[9]. Indeed, ABCC (dys)functions might be associated with tumour multidrug resistance and drug-drug interactions given the competitive affinity between substrates, with a possible clinical impact.

The structural resolution of ABC transporters has been an active field of research, leading to the elucidation of several conformations, namely inward-facing (IF), outward-facing (OF), and unlock-returned (UR) turnover conformations. These conformations illustrate the alternating access mechanism[10,11] required for large-scale conformational transitions[1,6,7,12] along the transport cycle. Recently, structural and functional diversity of ABC transporters has led to a fold-based classification[13], in which ABCC family is classified as type IV fold[2]. ABCC family members are single proteins comprising two transmembrane domains (TMDs) consisting of six transmembrane helices (TMHs). TMDs are connected to evolutionary conserved cytosolic nucleotide binding domains (NBDs). Several bovine ABCC1/MRP1 functional conformations were resolved[6,7,12] by cryogenic electron microscopy (cryo-EM). Namely, the structures of IF apo (PDB ID: 5UJ9[6]), IF substrate-bound (PDB ID: 5UJA[6]) as well as both the pre- and post-hydrolysis states under OF conformation (PDB IDs: 6BHU[7] and 6UY0[12], respectively) were resolved, providing an overview of large-scale transitions occurring along the transport cycle. We recently investigated *b*MRP1 conformations in various lipid bilayer models by molecular dynamics (MD) simulations, suggesting that the NBD asymmetry is key in ATP and substrate-binding events as well as in the allosteric communication between nucleotide binding sites (NBSs) and substrate-binding pocket[14]. Furthermore, the interplay between *b*MRP1 and lipid bilayer models was also investigated, suggesting an active role of the surrounding lipids in the IF-to-OF transition of *b*MRP1, and highlighting direct interactions between phosphatidylethanolamine lipids and cholesterol molecules. Such lipids were shown to actively participate in the distance communications between NBSs and the substrate-binding pocket[10,14]. However, focus was mostly paid to the dynamics of milestone conformations along the IF-to-OF transition, prior to ATP-hydrolysis.

The transport cycle requires the binding of two ATP molecules which are pseudo-symmetrically sandwiched between NBDs. For each NBS, ATP molecule is docked between the A-, H-, D-, and Q-loops, and Walker A and B motifs of one NBD and the ABC signature motif and X-loop of the other NBD[15]. MRP1, as other MRPs, is NBS degenerate ATP transporter[15]. The Walker B catalytic glutamate, A-loop aromatic binding tyrosine, and the first ABC signature glycine residues of non-canonical NBS1 are mutated into aspartate (Asp693), tryptophan (Trp653), and valine (Val1432) residues[15], respectively. This has been proposed to lead to a larger ATP affinity but also to a lower hydrolysis activity, as compared to the consensus NBS2[1,15]. After the substrate release, ATP-hydrolysis has been shown to be key to trigger the OF-to-IF large-scale conformational transition, in which signal transduction from NBDs to TMDs was suggested to occur through coupling helices[7,16]. In NBS degenerate ABC transporters, it is globally accepted that the presence of the functional and canonical NBS2 should ensure the ATP-hydrolysis and subsequent γ-phosphate release suspected to be required to reset the IF conformation[15,17,18]. However, MRP1 cryo-EM resolved structures for pre- and post-hydrolysis functional states do not exhibit significant structural differences. This suggests, altogether with single molecular FRET experiment, that NBD dimer dissociation is the OF-to-IF transition limiting event, but more surprisingly, ATP-hydrolysis and phosphate release might not induce conformational rearrangements in *b*MRP1, in contrast to other ABC transporters[12]. Therefore, this highlights that, even though general trends can be proposed for NBS degenerate ABC transporters, subtle differences between them may lead to different molecular mechanisms[1,15].

We here use μs-scaled MD simulations to investigate the structure and dynamics of *b*MRP1 in pre- and post-hydrolysis functional states. In line with our previous study, we built an OF *b*MRP1-ATP-ADP model embedded in different simplistic lipid bilayer models based on POPC (1-palmitoyl-2-oleoyl-sn-glycero-3-phosphocholine), POPE (1-palmitoyl-2-oleoyl-sn-glycero-3-phosphoethanolamine), and cholesterol; namely, POPC pure, POPC:Chol (3:1) and POPC:POPE:Chol (2:1:1). The present work aims to investigate the slight but likely relevant structural differences between pre- and post-hydrolysis states of OF conformations as well as the interactions between MRP1 and surrounding lipid molecules. It is important to note that in the present study, since the TMD_0 was not included in our model, TMH labelling use the short MRPs, i.e., from TMH1 to TMH12 to ease up comparison with other type IV fold ABC transporters.

2. Materials and Methods

2.1. Construction of pre- and post-hydrolysis *b*MRP1 models embedded in different lipid bilayer membranes

MD simulations performed for the pre-hydrolysis state, namely OF *b*MRP1-$(ATP)_2$ were taken from our previous work[14]. In the present study, the post-hydrolysis state (namely OF *b*MRP1-ATP-ADP) was built adopting the exact same protocol[14]. Shortly, initial models were built using the available resolved cryo-EM structures of OF *b*MRP1-$(ATP)_2$ (PDB ID: 6BHU[7]) and OF *b*MRP1-ATP-ADP-bound (PDB ID: 6UY0[12]). Engineered EQ mutation experimentally used to lower the rate of ATP-hydrolysis was manually reverted. Since the so-called "TMD_0" has been shown not to be involved in *b*MRP1 transport cycle[6,7,19], it was not included in the models. The pre-TMH1 lasso domain (L_0) has been shown to be mandatory for MRP1 function[1,6,20]; however, it was not totally resolved in the cryo-EM structures. Therefore, the missing parts of L_0 as well as the missing loop between TMH6 and NBD1 were modelled using Modeller v9.23[21]. L_0 domain was built based on the sequence but also using the IF L_0 domain as template (Supplementary Table 1). To avoid unphysical steric clashes, final models were shortly minimized in vacuum using Amber package[22,23] prior to be embedded in lipid bilayers. Protonation states of titratable residues were assigned by using the PROPKA software[24], while histidine residues were protonated after careful visual inspection of possible H-bond networks.

The OF *b*MRP1 ATP-ADP-bound structure was embedded into three different lipid bilayers, namely POPC pure, POPC:Chol (3:1), and POPC:POPE:Chol (2:1:1), using the CHARMM-GUI input generator[25,26] and *b*MRP1 coordinates from the OPM (Orientations of Proteins in Membranes) database[27] as z-alignment template. The three co-resolved cholesterol molecules were systematically kept in the two structures during all simulations. Among the used lipid bilayer models, POPC:POPE:Chol (2:1:1) mixture is considered the closest to model cell membranes. The other membrane compositions were used to investigate the protein-lipid interplay. The original total size of the system was *ca.*120 x 120 x 180$Å^3$ (Supplementary Table 2). To mimic physiological conditions, 0.15 M NaCl salt concentration was used, and the system was solvated with explicit water molecules[28]. The final systems are made of *ca.* 245 000 atoms (Supplementary Table 3).

2.2. Molecular dynamics simulations

CHARMM-GUI[25,26] outputs were converted to Amber format using charmmlipid2amber.py and pdb4amber AmberTools scripts[23,29]. Nucleotides and Mg^{2+} ions were added after building the protein-lipid systems; therefore, neutrality was ensured by randomly removing the corresponding number of counterions. Amber software was used to run simulations, as it was done previously[14]. Protein, lipid, water, and ions were modelled using respectively the FF14SB[30], Lipid17[31], TIP3P[28,32,33] forcefields, and monovalent and divalent ion parameters from Joung and Cheatham[34,35]. ATP and ADP parameters were derived from the Amber database available in http://amber.manchester.ac.uk/[36,37].

For all simulations, periodic boundary conditions were applied. The cut-off for non-bonded interactions (both Coulomb and van der Waals potentials) was 10 Å. Long-range electrostatic interactions were computed using the particle mesh Ewald method[38]. Amber18 and Amber20 packages[23,29] using CPU and GPU PMEMD codes were applied for minimization and MD simulations. Each system was initially minimized using four steps protocol, minimizing: (i) water O-atoms (20000 steps); (ii) all bonds involving H-atoms (20000 steps); (iii) water molecules and counterions (50000 steps) and (iv) the whole system (50000 steps). Thermalization to 310 K was carried out in two steps: (i) under (N,V,T) ensemble conditions, water molecules were thermalized to 100 K during 50 ps using 0.5 fs time integration; (ii) under semi-isotropic (N,P,T) ensemble conditions, the whole system was thermalized from 100 K to 310 K during 500 ps with 2 fs timestep. Each system was finally equilibrated using Berendsen barostat during 5 ns under (N,P,T) ensemble conditions with 2 fs timestep in semi-isotropic conditions. MD production runs were carried out with 2 fs integration timestep under (N,P,T) ensemble conditions with semi-isotropic scaling for 1.5 µs, except for OF *b*MRP1 ATP_2-bound in POPC:POPE:Chol (2:1:1) bilayer which reached 2 µs. Langevin dynamics thermostat[39] with 1.0 ps^{-1} collision frequency was used to maintain the temperature, while either Berendsen barostat[40] or Monte Carlo barostat[41] with semi-isotropic pressure scaling were applied to keep the constant pressure set at 1 bar respectively for OF *b*MRP1-$(ATP)_2$ and OF *b*MRP1-ATP-ADP systems. The latter was used to speed up computational time after ensuring that system box sizes were sufficiently equilibrated. Snapshots were saved every 100 ps. For each system, three replicas were performed in parallel from the thermalization step to better sample the local conformational space.

2.3. Analysis and visualization

The same analysis techniques were used to monitor the simulations as previously[14]. Analyses were performed using the CPPTRAJ[42] package and in-house Python scripts taking advantage of the MDAnalysis module[43,44] and the matplotlib v3.3.1 package[45]. Structure visualization and rendering were prepared using the VMD software (v1.9.3 and alpha-v1.9.4)[46]. Analyses were performed only on the equilibrated part of the MD simulations, *i.e.*, considering the last 800 or 400 ns shown on RMSD profiles reported Supplementary Fig. 1-2.

The so-called ABC structural parameters[17,47] were calculated (Supplementary Fig. 3-7) and used to map the ABC conformational space (Supplementary Fig. 8-9, Fig. 1a) as defined previously[14], following the work from Hofmann *et al.*[17] regarding IC angle, EC angle, EC distance and NBD distance as well as the former study carried out by Moradi *et al*. for NBD twist[48]. The GMM-based InfleCS[49,50] clustering method was used to map the subspace conformation free energy surfaces (Fig. 1b, Supplementary Fig. 10). The grid size was set at 80 point per variable, and 2 to 12 gaussian components for each GMM were considered to fit

densities. GMM functions were obtained by considering a maximum of 20 iterations. Free energy surfaces were calculated using the ABC structural parameters as structural determinants. Since the relevance of InfleCS[49,50] approach strongly relies on the quality of sampling during MD simulations, InfleCS[49,50] here only pictures the free energy landscape around the sampled local minima. As previously achieved[14], the relevance of InfleCS for OF *b*MRP1-ATP-ADP was monitored by calculating convergence profiles for each structural parameter separately (Supplementary Fig. 11). H-bond analyses (Fig. 2b, Supplementary Fig. 12) using 3.5 Å and 120° cutoffs respectively for distance and angle were performed by CPPTRAJ[42]. Contacts between the nucleotides and their binding site were calculated (Supplementary Fig. 13). Leaflet dependent lipid densities were calculated (Supplementary Fig. 14-16) as previously[14], *i.e.*, using the grid keyword in CPPTRAJ[42] concentrating on polar head lipids (PE or PC) or cholesterol OH-group. Focus was paid only to the high-density polar head region obtained from lipid bilayer models [46,51].

Allostery network pathways, as previously[14], were determined using the Allopath approach developed by Westerlund *et al*.[52,53]. Distant "communication efficiency" between two domains was obtained from the contact map and the mutual information matrix of protein residues and non-protein interactors such as surrounding lipid and bound nucleotides. With such an approach, a betweenness profile pictures (Supplementary Fig. 17-19) the involvement of each component (*i.e.*, residue, lipid, and nucleotide). For each lipid molecule, three nodes were defined corresponding to the polar head group and the two lipid tails. ATP and ADP were also split into three nodes: purine and ribose moiety as well as phosphate tail. Mg^{2+} ions and cholesterol molecules were considered as one node each. Allosteric pathways were calculated from extracellular regions (TMH1, 2, 10 and 11 and TMH4, 5, 7 and 8) to each NBD, separately, as defined in Supplemental Table 4.

3. Results

3.1. MD simulations reveal slight but relevant structural differences between the pre- and post-hydrolysis states

In the present section, particular attention is paid to MD simulations performed in POPC:POPE:Chol (2:1:1). Conformational spaces sampled for pre- and post-hydrolysis states (namely OF *b*MRP1-$(ATP)_2$ and OF *b*MRP1-ATP-ADP) were examined focusing on key ABC structural parameters (Fig. 1 and Supplementary Fig. 3-7). NBD distances and intracellular (IC) angles were used to monitor the intracellular opening, while the extracellular angle (EC) was used to assess the opening towards the external cell compartments. NBD rocking-twist as originally defined by Moradi *et al.*[47] was also monitored. These parameters were projected onto the ABC conformational space defined by measuring ABC structural parameters of a

large data set of experimentally resolved ABC transporters (Fig. 1a, Supplementary Fig. 8-9). The so-called inward-facing (IF), outward-facing (OF) and asymmetric unlock-returned (UR) turnover[17] states are explicitly separated using these structural parameters. For both pre- and post-catalytic states, IC angle shows similar trends picturing small IC opening, values ranging from 19.4 to 22.6°. Furthermore, they did not show large variability suggesting stable conformations (Fig. 1a, Supplementary Fig. 3). On the other side of the membrane, post-hydrolysis state exhibits smaller EC angle values than pre-catalytic states, ranging from 13.8 to 23.6 and from 12.6° to 19.3°, respectively for pre- and post-catalytic states. This is in line with the expected sealing of EC gate which is favoured after ATP-hydrolysis. EC opening variability is larger than for IC angle depicting the expected NBD locked conformation (Fig. 1a, Supplementary Fig. 3-4).

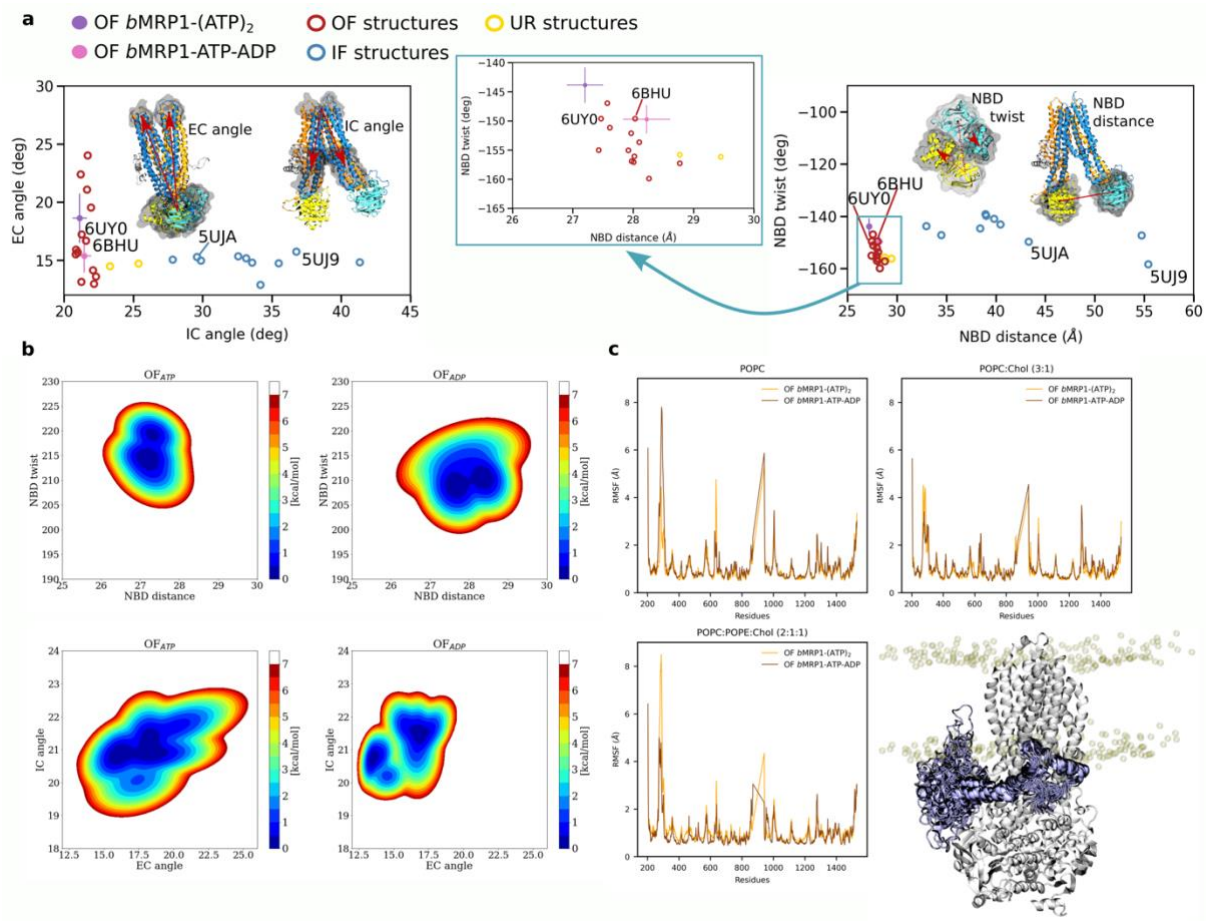

Figure 1. Structural dynamics of OF pre- and post-hydrolysis states. a) Projection of *b*MRP1 structural parameters of the pre- and post-hydrolysis states, respectively OF-$(ATP)_2$ and OF-ATP-ADP simulations, onto the ABC conformational space obtained from multiple resolved ABC structures. Each replica was averaged over the last 800 ns. PDB IDs of the resolved *b*MRP1 cryo-EM structures are explicitly mentioned. The zoom shows the OF area of the NBD twist – NBD distance plot. The first and second TMDs are respectively depicted in orange and blue, and NBD1 and NBD2 are respectively coloured yellow and cyan. **b)** System-dependent local conformational landscapes obtained from the GMM-based approach developed in the InfleCS method[49,50] highlights the influence of nucleotides on *b*MRP1 structural dynamics. **c)** RMSF calculated on the last 400 ns and structure representation of OF *b*MRP1-ATP-ADP POPC:POPE:Chol (2:1:1) show the L_0-dynamics.

Pre- and post-catalytic states mostly differ in the NBD dimer arrangement. The NBD rocking-twist angle of the post-hydrolysis state does not deviate from the originally resolved structure, while the NBD distance value is slightly larger (Fig. 1a, Supplementary Fig. 6-7). The opposite trend was observed in pre-catalytic state for which NBDs get closer to each other in MD simulations with respect to the cryo-EM resolved structure. This might be explained by stronger NBD-NBD non-covalent interactions in biomimetic membranes compared to detergent, as suggested in our previous work[14]. Furthermore, the E1454Q mutation used for cryo-EM resolution may also alter ATP-binding in NBS2. Interestingly, the post-catalytic OF *b*MRP1-ATP-ADP state exhibits a lower NBD twist than the pre-catalytic state by *ca.* 5°. Noteworthy, the post-hydrolysis state which is expected to be before the OF-to-IF transition is getting closer to the conformational space of the UR structures which were resolved in native nanodisk environment. This is in agreement with the recent structural findings suggesting that ABC transporter might adopt UR state prior to get back to IF conformational state, resetting the transport cycle[17]. However, the use of NBD distances should be carefully considered, especially, for NBD degenerate ABC transporters such as MRP1, given the expected pivotal role of ATP-bound NBS1 in maintaining NBD dimerization along the transport cycle[15], in agreement with our previous findings[14].

Assuming that our MD simulations were long enough to independently sample the local conformational subspace of pre- and post-catalytic metastable states, local free energy surfaces were calculated according to ABC structural parameters using the InfleCS framework[49,50] (Fig. 1b, Supplementary Fig. 10). Particular attention was paid to NBD structural parameters. Interestingly, two main populations were captured from MD simulations performed on the post-catalytic OF *b*MRP1-ATP-ADP state regarding NBD distance, showing a slightly larger flexibility in terms of NBD opening while it is unlikely to happen in pre-catalytic state. Likewise, a small difference for NBD rocking-twist parameter between pre- and post-hydrolysis states is captured from the free energy point of view, confirming that ATP-hydrolysis shifts the free energy surface toward more open and less twisted NBD dimer conformation. On the other side of the membrane, pre-hydrolysis state simulations show more flexible EC opening compared to the post-catalytic state. MD simulations performed on OF *b*MRP1-ATP-ADP state surprisingly suggest two well-separated populations. Interestingly, transition from one to the other requires crossing a relatively high energy barrier (*ca.* 3 kcal.mol^{-1}). Our simulations suggest that such transition may be favoured by slightly closed IC gate. However, this should be carefully considered and confirmed by further investigations.

Particular attention was also paid to the lasso domain (L_0) which connect the TMD_0 and the functional core of MRP1. It is worth remembering that TMD_0 was not included in the MRP1

model since it was shown not to be involved in the transport function[6,7,19]. However, experiments stressed out that L_0-less MRP1 is not functional[1,6,20]. MD simulations reveals large flexibility of the L_0 domain as pictures by monitoring root-mean-square deviation (RMSD) for the whole protein along the simulations (Supplementary Fig. 1). This was confirmed by assessing RMSD only on the ABC core (*i.e.*, extruding L_0) showing much smaller deviations along the simulations of pre- and post-catalytic states (Supplementary Fig. 2). Domain flexibilities were also assessed by measuring the per-residue root-mean-square fluctuations (RMSF) over the last 400 ns (Fig. 1c). Interestingly, RMSF analyses suggest higher flexibility for the pre-hydrolysis state in membranes containing cholesterol (Fig. 1c). Interestingly, in both pre- and post-catalytic states, L_0 flexibility suggests two distinct behaviours (Fig. 1c, Supplementary Fig. 20). On one hand, Asn203-Lys267 region does not exhibit large flexibility, remaining in close contact with pre-TMH1, TMH1, TMH2, TMH10, and TMH11. On the other hand, Ser268-Lys307 region displays larger variability. This agrees with the resolved structure since the latter has not been totally resolved by cryo-EM techniques. MD simulations also suggest that the flexible L_0-subdomain may interact with NBD1, even though L_0 roughly maps the same space in the pre- and post-hydrolysis states.

3.2. Differences in the nucleotide-binding of the pre- and post-hydrolysis states

As NBD distance and NBD twist values showed differences in the pre- and post-hydrolysis states, special attention was paid to the NBSs. MRP1 belongs to NBD degenerate ABC transporters of which NBS1 is expected to exhibit (i) increased important ATP-binding but (ii) significantly lower ATP-hydrolysis rate. Local key distances proposed to maintain the nucleotide in the binding site[14,54] were monitored between either ATP or ADP molecules and well-known conserved motifs (Fig. 2a). Distances between ATP molecules and NBS1 binding motifs are globally conserved when comparing pre- and post-hydrolysis states. Only the distance between A-loop Trp653 and adenosyl moiety is slightly larger in the post-hydrolysis state by *ca.* 1.0 Å. This is in agreement with former observations made on NBD degenerate ABC transporters suggesting that ATP remains constantly bound in NBS1 along several transport cycles[15]. In contrast, all distances between the nucleotide and NBS2 motifs differ. The most important deviation is observed with the Q-loop motif (respectively 6.2 ± 0.1 and 8.9 ± 0.8 Å in pre- and post-hydrolysis states). H-loop and Walker B motifs also show significant structural differences. This might be easily explained by the absence of γ-phosphate which is supposed to bind the Q-loop motif. However, in presence of ADP in NBS2, motifs supposed to bind γ-phosphate tend anyway to locally reshape by getting closer to β-phosphate moiety (*e.g.*, ABC signature, H-loop, and Walker B), as shown by distances measured with terminal β-phosphate O-atom (d^*_{post} in Fig. 2a). This suggests a local rearrangement of NBDs after ATP-hydrolysis.

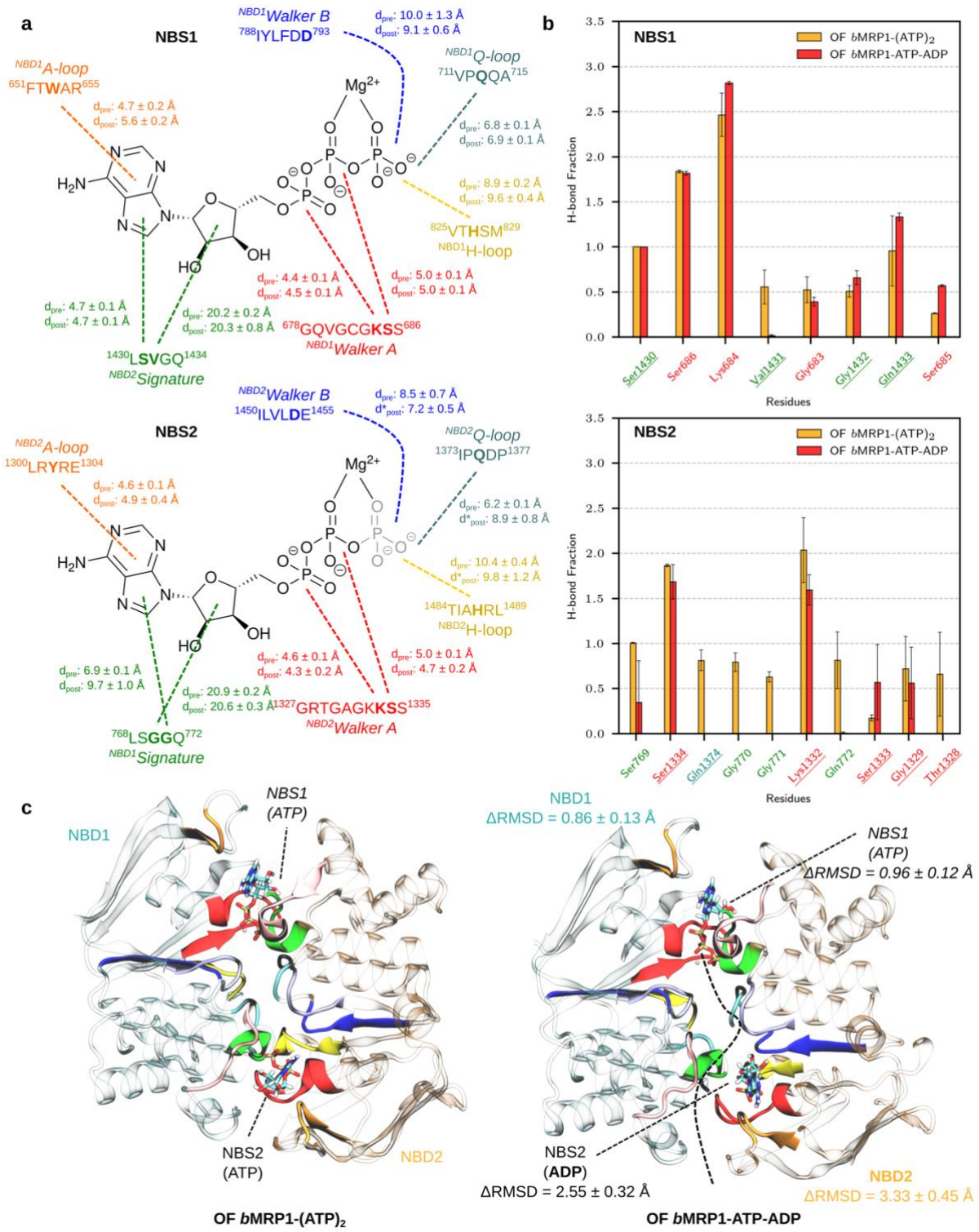

Figure 2. Nucleotide-binding sites in the pre- and post-hydrolysis states of OF *b*MRP1. a) Important distances between the nucleotides and key residues in the nucleotide-binding sites. **b)** Calculated H-bond networks between nucleotides and NBS1 (top) or NBS2 (bottom). **c)** ΔRMSD of NBD1, NBD2 and NBS1, NBS2 of the post-hydrolysis state compared to the pre-hydrolysis state. The post-hydrolysis state is more open as it is indicated by the dashed line. Conserved motives are coloured as follows: Walker A red, Walker B blue, signature motif green, A-loop orange, Q-loop teal, X-loop pink, D-loop cyan, and H-loop yellow.

More specifically, binding modes of the nucleotides were also investigated by assessing atomic contacts, H-bond networks as well as van der Waals and Coulomb potentials between ATP or ADP molecules and NBS motifs (Fig. 2b, Supplementary Fig. 12-13, 21). It must be stressed that van der Waals and Coulomb potentials can only provide qualitative hints to compare the binding sites due to a compensation of errors between the two potentials especially at short distances[55]. H-bond fractions (Fig.2b) highlights the significant difference between pre- and post-hydrolysis in NBS2 H-bond network, especially regarding the ABC signature motif and Q-loop. This is confirmed by interatomic contact analyses since there are significantly less contacts in the post-hydrolysis state in NBS2. Walker A motif in NBS2 has slightly looser connections with ADP than ATP, which might be involved in the subsequent nucleotide release. NBS-nucleotide atomic contact fraction maps confirm weaker interactions between ADP and NBS2 ABC signature motif and Q-loop, while contacts remain similar with other motifs (Supplementary Fig.13). Interestingly, ABC signature motif has similar H-bond fraction in NBS1 in pre- and post-hydrolysis states. NBS1 Walker A motif, that binds α- and β-phosphates, exhibits slightly stronger connections in the post-hydrolysis state in agreement with the expected maintain of ATP molecule along likely multiple transport cycles[15].

NBS structural differences between pre- and post-hydrolysis states are expected to modulate the NBD dimer supramolecular arrangement. In this context, NBD2 arrangement with respect to NBD1 were assessed by calculating ΔRMSDs focusing on NBDs either separately or using NBD1 position as reference over the trajectories. Interestingly, NBD1 secondary structure is conserved during the hydrolysis (ΔRMSD being 0.86 ± 0.13 Å, see Fig. 2c). NBD2 secondary structure deviates slightly more while comparing pre- and post-hydrolysis (ΔRMSD being 1.36 ± 0.12 Å). However, NBD1-aligned structure clearly highlights the structural deviation of post-catalytic NBD dimer as compared to pre-catalytic state. The pivotal role of NBS1 is confirmed as well as the asymmetric NBD motion along the transport cycle[15]. For instance, NBD2 and NBS2 exhibit larger ΔRMSD values, respectively 3.33 ± 0.45 Å and 2.55 ± 0.32 Å. Moreover, visual inspection clearly underlines the opening of NBD dimer on the side of NBS2, as previously suggested[14]. However, as expected, no NBD dimer dissociation event was observed in MD simulations for post-catalytic states in any of the simulations conducted independently on the lipid bilayer (Fig. 1a, Supplementary Fig. 8-9).

3.3. Protein-Lipid interactions

As observed for IF states[14], lipid components only slightly affect the structure close to the local equilibrium subspace. Regardless of membrane composition, local free energy minima obtained from the InfleCS[49,50] approach (Fig.1a, Supplementary Fig. 10) are located in similar regions of the ABC conformational subspace. Interestingly, in PE free lipid bilayer models, MD

simulations suggest larger protein variability, especially for the EC angle, as compared to MD simulations performed in POPC:POPE:Chol (2:1:1) lipid bilayer (Supplementary Fig. 10). Likewise, H-bond analyses showed that NBS nucleotide binding modes is not strongly affected by lipid bilayer composition. In post-hydrolysis states, ADP is less bound to NBS2 regardless of membrane composition as pictured by overall calculated H-bond fractions between nucleotide and NBS residues, as well as by monitoring non-covalent interaction energies along MD simulations (Fig. 2b and Supplementary Fig. 12-13).

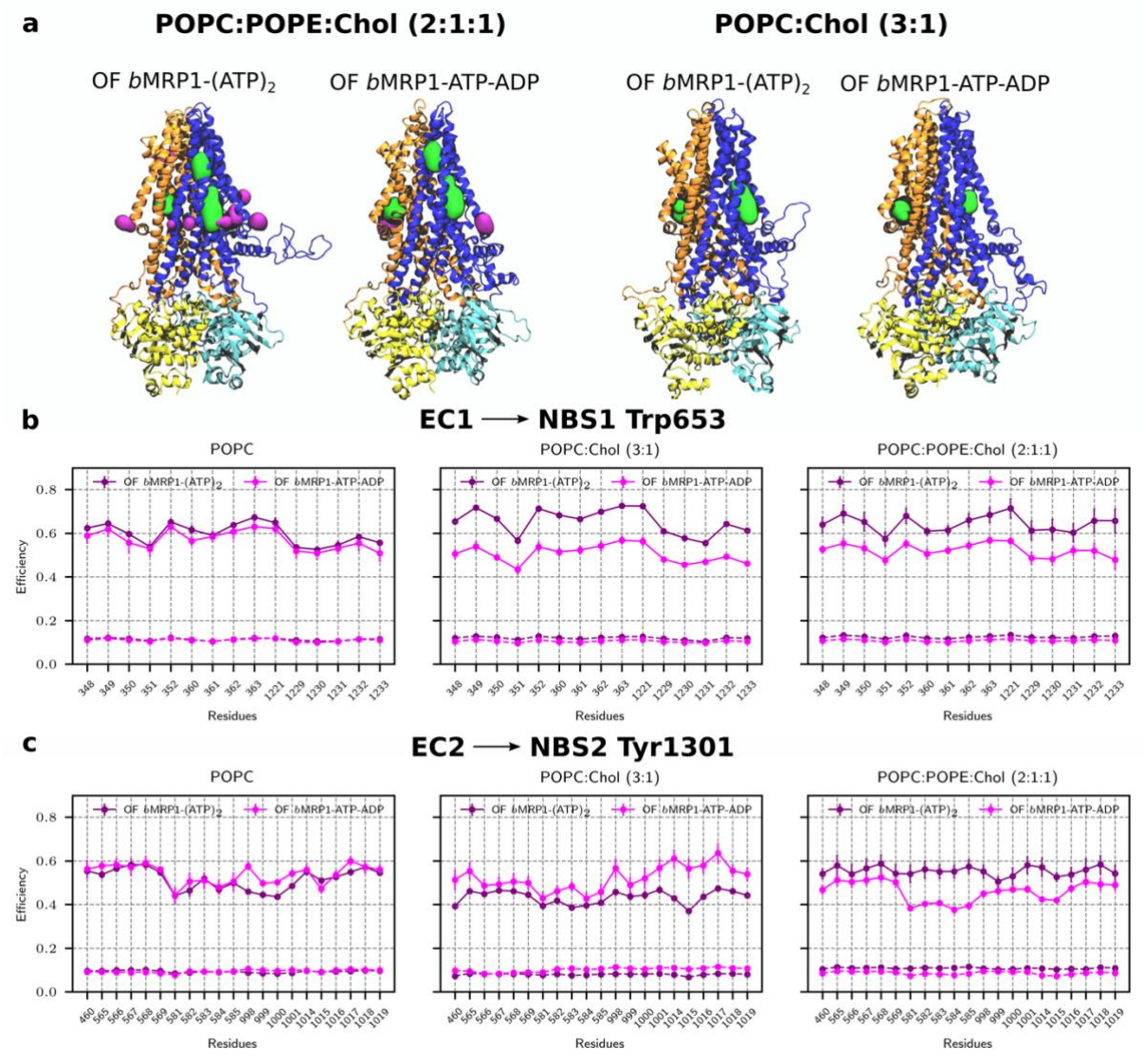

Figure 3. The role of the lipids on the dynamics of the pre- and post-hydrolysis states. a) Key lipids, cholesterol (green) and PE lipid (magenta) hotspots defined by presence likelihood higher than 50%. **b)-c)** Allosteric efficiency from the EC regions to the NBS A-loop aromatic residues.

Overall dynamic cross-correlation between residues show less correlation in the post-hydrolysis state in POPC:POPE:Chol (2:1:1) membrane; however, this difference is not

observable in pure POPC and POPC:Chol (3:1) lipid bilayers (Supplementary Fig. 22). Cryo-EM OF structures were resolved including three cholesterol molecules that were suggested to actively participate in the allosteric communication between substrate binding pocket and NBD. As observed for pre-hydrolysis state, resolved cholesterol remains in close contact with pre-TMH7 elbow helix all along the simulation (Fig. 3a). Interestingly, MD simulations reveal plausible PE binding spots. It shed light on key PE-protein H-bond interactions and thus hotspots which are observed in the lower leaflet. This is in agreement with the known *in vivo* asymmetry for cell membrane composition, since PE lipids are mostly located in the lower leaflet than the upper leaflet. However, PE-binding seems to be more favourable prior to ATP-hydrolysis, even though such assumptions should be considered carefully given that the timescale is not sufficient to provide an accurate sampling of surrounding lipid motions.

Allosteric communications between EC regions and NBS A-loop aromatic residues (namely Trp653 and Tyr1301 for NBS1 and NBS2, respectively) were assessed by calculating the efficiency. Distant communications were monitored by considering two distinct EC regions from TMH bundles (*i.e.*, EC regions for TMH1, 2, 10 and 11 and for TMH4, 5, 7 and 8) since they were shown to be responsible for the EC opening[17]. As previously reported[10,14], MD simulations confirmed the central role of lipid membrane in participating in the allosteric communication between cytosolic domains and EC region of TMHs (Fig. 3b-c, Supplementary Fig. 23). This confirmed that surrounding lipids participate in propagating dynamics along the transporter. This was also confirmed by calculating the lower information flows (or betweenness) across the protein residues in presence of surrounding lipids as compared to those of the protein alone (Supplementary Fig. 17-19). However, no significant difference was observed regarding the impact of the bilayer composition.

4. Discussion

*b*MRP1 is the only drug exporter in ABCC family for which there are resolved cryo-EM structures available, so far. The ITC[5,9,56] has stressed out their clinical and pharmacological relevance. Knowledge about MRP1 dynamics and functions is still fragmented, in contrast to its cousin ABCB1/P-gp. In the present work, all-atom MD simulations were performed in the pre- and post-hydrolysis states, respectively OF *b*MRP1-$(ATP)_2$ and OF *b*MRP1-ATP-ADP, in different bilayers including PC and PE lipids as well as cholesterol, to compare their dynamics and structures.

Global conformational dynamics in POPC:POPE:Chol (2:1:1) show unfavourable EC opening, smaller NBD twist, and higher NBD distance indicating that the post-hydrolysis state adopts a close-conformation rather than an outward-open conformation. EC closing and IC opening are likely necessary for the OF-to-IF conformational changes. Present results as well as our

previous studies[14] clearly indicate that outward-facing open conformation is a transient state which may exist only for the substrate release. We here therefore suggest that the use of "OF" conformation for such states should perhaps be replaced by the so-called "close-conformation" (cc) as stated for ABCB4[57]. It is worth mentioning, that only a few IV-fold ABC transporters were resolved with a clear open OF conformation (*e.g.*, the historical Sav1866[58]) as shown in Supplementary Fig. 24.

Our present work also highlights the structural dynamics of the L_0 domain. MD simulations suggest the existence of a dynamic interaction with NBD1, which tends to be more pronounced in the post-hydrolysis state. Even though no clear clue was obtained to better understand its role, previous experiments have shown that the lasso motif is required for MRP1 function[1,6,20]. Surprisingly, it has been shown that co-expression of L_0 is however sufficient for substrate transport by MRP1[6]. Altogether with our present results, this may suggest that simply the L_0-NBD1 non-covalent interactions may play a role in triggering the OF-to-IF large scale conformational changes. However, such assumption will require further joint experimental and computational investigations.

Particular attention has been paid to the NBDs. NBD rocker-switch angle slightly but significantly deviate by *ca.* 5° between pre- and post-hydrolysis states. In agreement with structural insights observed in P-gp, hydrolysis induces local conformational changes in the conserved motifs, mostly in the signature motif[59]. This is in agreement with P-gp for which two EC opening main populations were observed depending on A-loop position[11]. However, in MRP1, calculated EC opening deviation remains lower than in P-gp. This might be explained by a different inherent behaviour of MRP1, which may be more pronounced owing to the fact the NBD1 is degenerated. Indeed, as shown in our former study[14], NBD1 coupling helix does not adopt the "ball-and-socket" conformation, leading to a lower transduction signal from NBD to TMDs. Our present calculations also confirm that ATP-binding in NBS1 acts likely as pivot since NBD1 and NBS1 are almost structurally identical regardless of the hydrolysis state. NBD2 exhibit pseudo-asymmetric structural deformation on the NBS2 side after ATP-hydrolysis. This was confirmed by the monitoring of the local distances, as well as non-covalent interactions between the nucleotides and the protein (including H-bond, van der Waals and Coulomb potentials) that suggest stronger interaction between the ATP and conserved motifs in NBS1 than in NBS2 even in the post-hydrolysis state. This strengthens the hypothesis suggesting that ATP release from NBS1 is unlikely even during several transport cycles[15]. Finally, our present MD simulations also strengthen the expected central role of PE lipids in the inner leaflet as well as cholesterol in the so-called Cholesterol recognition amino acid consensus (CRAC) or inverted (CARC) motifs. Indeed, these motifs

were also observed in other ABC transporters as well for MRP1[60]. However, their exact roles still require to be elucidated.

5. Acknowledgements

We thank Xavier Montagutelli from the IT department of Limoges University for technically supporting supercomputer facilities. Calculations were performed using CALI ("CAlcul en LImousin") and “Baba Yaga” supercomputers hosting in Limoges University, as well as on the “Jean-Zay” national supercomputer from IDRIS HPC resources under the allocations 2020-A0080711487, 2021-A0100711487 and 2022-A0120711487 made by GENCI. This work was supported by grants from the “Agence Nationale de la Recherche” (ANR-19-CE17-0020-01 IMOTEP and ANR-21-CE18-0030 RAPRACLID), Région Nouvelle Aquitaine and “Institut National de la Santé et de la Recherche Médicale” (INSERM, AAP-NA-2019-VICTOR).

6. Conflict of Interest Statement

The authors declare no competing interests.

7. Authorship

Á.T and F.D.M conceived the study. Á.T and F.D.M. conducted all the simulations. Á.T, A.J., V.C and F.D.M analysed the simulations. Á.T. and F.D.M. interpretated the results and discussed them together with A.J. and V.C. Á.T. and F.D.M wrote the manuscript, and it was edited, reviewed, and approved by all authors.

8. Data availability

All data analysed during this study are included in this published article (and its supplementary information files). Only the MD trajectories are available upon reasonable requests.

9. References

1. Kroll, T., Prescher, M., Smits, S. H. J. & Schmitt, L. Structure and Function of Hepatobiliary ATP Binding Cassette Transporters. *Chem. Rev.* **121**, 5240–5288 (2021).
2. Thomas, C. & Tampé, R. Structural and Mechanistic Principles of ABC Transporters. *Annu. Rev. Biochem.* **89**, 605–636 (2020).
3. Scortecci, J. F. *et al.* Cryo-EM structures of the ABCA4 importer reveal mechanisms underlying substrate binding and Stargardt disease. *Nat. Commun.* **12**, 5902 (2021).
4. Xu, D. *et al.* Cryo-EM structure of human lysosomal cobalamin exporter ABCD4. *Cell Res.* **29**, 1039–1041 (2019).

5. Zamek-Gliszczynski, M. J. *et al.* Transporters in Drug Development: 2018 ITC Recommendations for Transporters of Emerging Clinical Importance. *Clin. Pharmacol. Ther.* **104**, 890–899 (2018).
6. Johnson, Z. L. & Chen, J. Structural Basis of Substrate Recognition by the Multidrug Resistance Protein MRP1. *Cell* **168**, 1075-1085.e9 (2017).
7. Johnson, Z. L. & Chen, J. ATP Binding Enables Substrate Release from Multidrug Resistance Protein 1. *Cell* **172**, 81-89.e10 (2018).
8. The International Transporter Consortium *et al.* Membrane transporters in drug development. *Nat. Rev. Drug Discov.* **9**, 215–236 (2010).
9. Zamek-Gliszczynski, M. J. *et al.* Transporters in Drug Development: International Transporter Consortium Update on Emerging Transporters of Clinical Importance. *Clin. Pharmacol. Ther.* **112**, 485–500 (2022).
10. Immadisetty, K., Hettige, J. & Moradi, M. Lipid-Dependent Alternating Access Mechanism of a Bacterial Multidrug ABC Exporter. *ACS Cent. Sci.* **5**, 43–56 (2019).
11. Verhalen, B. *et al.* Energy transduction and alternating access of the mammalian ABC transporter P-glycoprotein. *Nature* **543**, 738–741 (2017).
12. Wang, L. *et al.* Characterization of the kinetic cycle of an ABC transporter by single-molecule and cryo-EM analyses. *eLife* **9**, e56451 (2020).
13. Thomas, C. *et al.* Structural and functional diversity calls for a new classification of ABC transporters. *FEBS Lett.* **594**, 3767–3775 (2020).
14. Tóth, Á., Janaszkiewicz, A., Crespi, V. & Meo, F. D. On the interplay between lipids and asymmetric dynamics of an NBS degenerate ABC transporter. 2022.05.16.492073 Preprint at https://doi.org/10.1101/2022.05.16.492073 (2022).
15. Stockner, T., Gradisch, R. & Schmitt, L. The role of the degenerate nucleotide binding site in type I ABC exporters. *FEBS Lett.* **594**, 3815–3838 (2020).
16. Göddeke, H. *et al.* Atomistic Mechanism of Large-Scale Conformational Transition in a Heterodimeric ABC Exporter. *J. Am. Chem. Soc.* **140**, 4543–4551 (2018).

17. Hofmann, S. *et al.* Conformation space of a heterodimeric ABC exporter under turnover conditions. *Nature* **571**, 580–583 (2019).

18. Prieß, M., Göddeke, H., Groenhof, G. & Schäfer, L. V. Molecular Mechanism of ATP Hydrolysis in an ABC Transporter. *ACS Cent. Sci.* **4**, 1334–1343 (2018).

19. Kroll, T., Prescher, M., Smits, S. H. J. & Schmitt, L. Structure and Function of Hepatobiliary ATP Binding Cassette Transporters. *Chem. Rev.* (2020) doi:10.1021/acs.chemrev.0c00659.

20. Bickers, S. C., Benlekbir, S., Rubinstein, J. L. & Kanelis, V. Structure of Ycf1p reveals the transmembrane domain TMD0 and the regulatory region of ABCC transporters. *Proc. Natl. Acad. Sci.* **118**, e2025853118 (2021).

21. Webb, B. & Sali, A. Comparative Protein Structure Modeling Using MODELLER. *Curr. Protoc. Bioinforma.* **54**, (2016).

22. Case, D. A. *et al.* AMBER 2020. (2020).

23. Case, D. A. *et al.* AMBER 2018.

24. Søndergaard, C. R., Olsson, M. H. M., Rostkowski, M. & Jensen, J. H. Improved Treatment of Ligands and Coupling Effects in Empirical Calculation and Rationalization of pKa Values. *J. Chem. Theory Comput.* **7**, 2284–2295 (2011).

25. Jo, S., Kim, T., Iyer, V. G. & Im, W. CHARMM-GUI: A web-based graphical user interface for CHARMM. *J. Comput. Chem.* **29**, 1859–1865 (2008).

26. Wu, E. L. *et al.* CHARMM-GUI *Membrane Builder* toward realistic biological membrane simulations. *J. Comput. Chem.* **35**, 1997–2004 (2014).

27. Lomize, M. A., Pogozheva, I. D., Joo, H., Mosberg, H. I. & Lomize, A. L. OPM database and PPM web server: resources for positioning of proteins in membranes. *Nucleic Acids Res.* **40**, D370–D376 (2012).

28. Price, D. J. & Brooks, C. L. A modified TIP3P water potential for simulation with Ewald summation. *J. Chem. Phys.* **121**, 10096–10103 (2004).

29. Salomon-Ferrer, R., Case, D. A. & Walker, R. C. An overview of the Amber biomolecular simulation package: Amber biomolecular simulation package. *Wiley Interdiscip. Rev. Comput. Mol. Sci.* **3**, 198–210 (2013).

30. Maier, J. A. *et al.* ff14SB: Improving the Accuracy of Protein Side Chain and Backbone Parameters from ff99SB. *J. Chem. Theory Comput.* **11**, 3696–3713 (2015).

31. Dickson, C. J. *et al.* Lipid14: The Amber Lipid Force Field. *J. Chem. Theory Comput.* **10**, 865–879 (2014).

32. Jorgensen, W. L., Chandrasekhar, J., Madura, J. D., Impey, R. W. & Klein, M. L. Comparison of simple potential functions for simulating liquid water. *J. Chem. Phys.* **79**, 926–935 (1983).

33. MacKerell, A. D. *et al.* All-atom empirical potential for molecular modeling and dynamics studies of proteins. *J. Phys. Chem. B* **102**, 3586–3616 (1998).

34. Joung, I. S. & Cheatham, T. E. Determination of Alkali and Halide Monovalent Ion Parameters for Use in Explicitly Solvated Biomolecular Simulations. *J. Phys. Chem. B* **112**, 9020–9041 (2008).

35. Joung, I. S. & Cheatham, T. E. Molecular Dynamics Simulations of the Dynamic and Energetic Properties of Alkali and Halide Ions Using Water-Model-Specific Ion Parameters. *J. Phys. Chem. B* **113**, 13279–13290 (2009).

36. Meagher, K. L., Redman, L. T. & Carlson, H. A. Development of polyphosphate parameters for use with the AMBER force field. *J. Comput. Chem.* **24**, 1016–1025 (2003).

37. Galindo-Murillo, R. *et al.* Assessing the Current State of Amber Force Field Modifications for DNA. *J. Chem. Theory Comput.* **12**, 4114–4127 (2016).

38. Darden, T., York, D. & Pedersen, L. Particle mesh Ewald: An N·log(N) method for Ewald sums in large systems. *J. Chem. Phys.* **98**, 10089–10092 (1993).

39. Davidchack, R. L., Handel, R. & Tretyakov, M. V. Langevin thermostat for rigid body dynamics. *J. Chem. Phys.* **130**, 234101 (2009).

40. Berendsen, H. J. C., Postma, J. P. M., van Gunsteren, W. F., DiNola, A. & Haak, J. R. Molecular dynamics with coupling to an external bath. *J. Chem. Phys.* **81**, 3684–3690 (1984).

41. Åqvist, J., Wennerström, P., Nervall, M., Bjelic, S. & Brandsdal, B. O. Molecular dynamics simulations of water and biomolecules with a Monte Carlo constant pressure algorithm. *Chem. Phys. Lett.* **384**, 288–294 (2004).

42. Roe, D. R. & Cheatham, T. E. PTRAJ and CPPTRAJ: Software for Processing and Analysis of Molecular Dynamics Trajectory Data. *J. Chem. Theory Comput.* **9**, 3084–3095 (2013).

43. Gowers, R. J. *et al.* MDAnalysis: A Python Package for the Rapid Analysis of Molecular Dynamics Simulations. *Proc. 15th Python Sci. Conf.* 98–105 (2016) doi:10.25080/Majora-629e541a-00e.

44. Michaud-Agrawal, N., Denning, E. J., Woolf, T. B. & Beckstein, O. MDAnalysis: A toolkit for the analysis of molecular dynamics simulations. *J. Comput. Chem.* **32**, 2319–2327 (2011).

45. Hunter, J. D. Matplotlib: A 2D Graphics Environment. *Comput. Sci. Eng.* **9**, 90–95 (2007).

46. Humphrey, W., Dalke, A. & Schulten, K. VMD: visual molecular dynamics. *J. Mol. Graph.* **14**, 33–38, 27–28 (1996).

47. Moradi, M. & Tajkhorshid, E. Mechanistic picture for conformational transition of a membrane transporter at atomic resolution. *Proc. Natl. Acad. Sci.* **110**, 18916–18921 (2013).

48. Moradi, M. & Tajkhorshid, E. Mechanistic picture for conformational transition of a membrane transporter at atomic resolution. *Proc. Natl. Acad. Sci.* **110**, 18916–18921 (2013).

49. Westerlund, A. M. & Delemotte, L. InfleCS: Clustering Free Energy Landscapes with Gaussian Mixtures. *J. Chem. Theory Comput.* **15**, 6752–6759 (2019).

50. Westerlund, A. M., Harpole, T. J., Blau, C. & Delemotte, L. Inference of Calmodulin's Ca2+-Dependent Free Energy Landscapes via Gaussian Mixture Model Validation. *J. Chem. Theory Comput.* **14**, 63–71 (2018).

51. Guixà-González, R. *et al.* MEMBPLUGIN: studying membrane complexity in VMD. *Bioinforma. Oxf. Engl.* **30**, 1478–1480 (2014).

52. Westerlund, A. M., Fleetwood, O., Pérez-Conesa, S. & Delemotte, L. Network analysis reveals how lipids and other cofactors influence membrane protein allostery. *J. Chem. Phys.* **153**, 141103 (2020).

53. Kang, P. W. *et al.* Calmodulin acts as a state-dependent switch to control a cardiac potassium channel opening. *Sci. Adv.* **6**, eabd6798 (2020).

54. Wen, P.-C., Verhalen, B., Wilkens, S., Mchaourab, H. S. & Tajkhorshid, E. On the Origin of Large Flexibility of P-glycoprotein in the Inward-facing State. *J. Biol. Chem.* **288**, 19211–19220 (2013).

55. Zgarbová, M., Otyepka, M., Šponer, J., Hobza, P. & Jurečka, P. Large-scale compensation of errors in pairwise-additive empirical force fields: comparison of AMBER intermolecular terms with rigorous DFT-SAPT calculations. *Phys. Chem. Chem. Phys.* **12**, 10476–10493 (2010).

56. Giacomini, K. M. *et al.* Membrane transporters in drug development. *Nat. Rev. Drug Discov.* **9**, 215–236 (2010).

57. Olsen, J. A., Alam, A., Kowal, J., Stieger, B. & Locher, K. P. Structure of the human lipid exporter ABCB4 in a lipid environment. *Nat. Struct. Mol. Biol.* **27**, 62–70 (2020).

58. Dawson, R. J. P. & Locher, K. P. Structure of a bacterial multidrug ABC transporter. *Nature* **443**, 180–185 (2006).

59. Dehghani-Ghahnaviyeh, S., Kapoor, K. & Tajkhorshid, E. Conformational changes in the nucleotide-binding domains of P-glycoprotein induced by ATP hydrolysis. *FEBS Lett.* **595**, 735–749 (2021).

60. Thangapandian, S., Kapoor, K. & Tajkhorshid, E. Probing cholesterol binding and translocation in P-glycoprotein. *Biochim. Biophys. Acta BBA - Biomembr.* **1862**, 183090 (2020).